

High energy properties of PKS 1830-211

Shu Zhang ¹, Yu-peng Chen ¹, Werner Collmar ², Luigi Foschini ³, Ti-Pei Li ^{1,4},
Diego F. Torres ⁵, Jian-Min Wang ^{1,6}

ABSTRACT

We report on an analysis of X- and γ -ray observations of PKS 1830 – 211, based on the long-term campaigns carried out by *INTEGRAL* and COMPTEL. The *INTEGRAL* data currently available present a 33σ significance detection in the 20 – 100 keV band, while the COMPTEL 6-years data provide a 5.2σ significance detection in the 1 – 3 MeV energy band. At hard X-rays, *INTEGRAL* and supplementary *SWIFT* observations show flux variability on timescales of months. At γ -rays, the source shows persistent emission over years. The hard X-ray spectrum is well represented by a power-law model, with $\Gamma \sim 1.3$ in the 20 – 250 keV band. This photon index is well consistent with the previous report of $\Gamma \sim 1.3$ obtained at $E > 3.5$ keV from the best fit of *XMM-Newton* data with a broken power law model. The joint *XMM-Newton/INTEGRAL* spectrum presented here is then fit with a broken power-law model and the parameters are refined compared to the previous. The results show the photon index changes from ~ 1.0 to ~ 1.3 at a break energy ~ 4 keV. At MeV energies, the spectrum softens to $\Gamma \sim 2.2$. These results, together with the EGRET measurement at $E \geq 100$ MeV, constitute a broad-band spectrum containing the peak of the power output at MeV energies, similar to most high-luminosity γ -ray blazars. The measured spectral characteristics are then discussed in the framework of the gravitational lens effects.

Subject headings: Quasars: general – Quasars: individual: PKS 1830 – 211 – X-rays: galaxies – Gamma-rays: galaxies

¹Key Laboratory for Particle Astrophysics, Institute of High Energy Physics, 19B YuQuan Road, Beijing 100049, China

²Max-Planck-Institut für Extraterrestrische Physik, P.O. Box 1603, 85740 Garching, Germany

³INAF/IASF-Bologna, via Gobetti 101, 40129, Bologna, Italy

⁴Center for Astrophysics, Tsinghua University, Beijing 100084, China

⁵ICREA & Institut de Ciències de l'Espai (IEEC-CSIC), Campus UAB, Facultat de Ciències, Torre C5-parell, 2a planta, 08193 Barcelona, Spain

⁶Theoretical Physics Center for Science Facilities (TPCSF), CAS.

1. Introduction

Since the first gravitational lens candidate was detected in 1979 (Walsh et al. 1979), the total number of such system has grown since (e.g. Schneider et al. 1992). Among them is the high redshift blazar PKS 1830 – 211 ($z = 2.507$), gravitationally lensed by an intervening galaxy at $z = 0.89$. The discovery of such gravitational system traces back to radio observations (Pramesh Rao & Subrahmanyam 1988). The radio map was composed of two compact components separated by $1''$, supposed to be the split images from the central region of the source and an extended structure which is most probably from the jet and regarded as an unusually strong Einstein ring (see Jauncey et al. 1991; Sunita Nair et al. 1993). Steppe et al. (1993) have shown that PKS 1830 – 211 is radio variable on timescales of months.

X-ray observations (*Chandra* and *INTEGRAL*) revealed a quite hard spectrum, modeled with a power-law with a photon index 1.09 ± 0.05 over the energy band $0.5 - 80$ keV (De Rosa et al. 2005). The spectral flattening at low energies has been often modeled with absorption in excess to the Galactic column ($N_{\text{H}} = 2.05 \times 10^{21} \text{ cm}^{-2}$, Kalberla et al. 2005). The column density has been measured at soft X-rays by *ROSAT* (Mathur & Nair 1997) and *ASCA* (Oshima et al. 2001) as well as by *Chandra* (De Rosa et al. 2005), which suggests a column density of either $\sim 10^{22} \text{ cm}^{-2}$ at the lensing galaxy ($z = 0.86$) or $\sim 10^{23} \text{ cm}^{-2}$ intrinsic to the source. *XMM-Newton* observations gave similar results, but the best fit is obtained with a broken power-law model, with the photon index changing from ~ 1.0 to ~ 1.3 at energies around 3.5 keV (Foschini et al. 2006).

PKS 1830 – 211 was included in the first *INTEGRAL* catalogue by Beckmann et al. (2006), with a photon index $1.96_{-0.24}^{+0.27}$ in the 20 – 100 keV energy band and in the *INTEGRAL* extragalactic survey by Bassani et al. (2006), with a 20 – 100 keV flux ~ 3 mCrab level averaged over the first 2.5 years of the *INTEGRAL* observations.

At MeV energies PKS 1830 – 211 was firstly reported by Collmar (2006). The COMPTEL first 4-year observations (1991-1995) revealed a detection of 4.5σ in the 1 – 3 MeV band. Contemporaneously, PKS 1830 – 211 was detected by EGRET at ≥ 100 MeV with 7.8σ significance and a photon index 2.59 ± 0.13 (Hartman et al. 1999).

Since the amount of *INTEGRAL* public data has been significantly increased after the last report, we decided to carry out a detailed analysis of PKS 1830 – 211 with all available *INTEGRAL* data. We also reanalyzed the *XMM-Newton* data with a newer software version, which allow us to extend the analysis down to 0.2 keV. The data from COMPTEL and EGRET are also reanalyzed and added in order to obtain the best broad-band high-energy spectrum available to date.

Long-term observations by *SWIFT* at hard X-rays and by COMPTEL at MeV energies are dug for investigating the spectral and flux variability. The results are finally discussed in the context of a gravitational lensing system, as is appropriate to PKS 1830 – 211.

In the following we assume $H_0 = 73.4 \text{ km s}^{-1} \text{ Mpc}^{-1}$ and $q_0 = 0$, measured from the latest *WMAP* data (Spergel et al. 2007).

2. Observations and data analysis

2.1. *INTEGRAL*

INTEGRAL is an ESA scientific mission dedicated to high-resolution spectroscopy ($E/\Delta E \simeq 500$; SPI see Vedrenne et al. 2003) and imaging (angular resolution: $12'$ FWHM, point source location accuracy: $\simeq 1' - 3'$; IBIS, see Ubertini et al. 2003) of celestial γ -ray sources in the energy range 15 keV to 10 MeV, with simultaneous monitoring at X-rays (3 – 35 keV, angular resolution: $3'$; JEM-X, see see Lund et al. 2003) and optical wavelength (Johnson V-filter, 550 nm; OMC, see see Mas-Hesse et al. 2003). All the instruments onboard *INTEGRAL*, except OMC, work with coded masks. The observational data from the detector IBIS/ISGRI (20 – 250 keV, Lebrun et al. 2003) have been considered in our analysis of PKS 1830 – 211, because of highest quality.

The available *INTEGRAL* observations when PKS 1830 – 211 fell into the Fully-Coded Field of View (FCFoV) of ISGRI (up to April 29, 2006; see Table 1) comprise about 1095 science windows (scw), for a total exposure of 2500 ks, i.e., about 550 ks of new data analyzed here for the first time. Most of these observations were carried out in a 5×5 dithering mode. The analysis were performed by using the *INTEGRAL* Offline Scientific Analysis (OSA) version 7.0, whose algorithms for IBIS are described in Goldwurm et al. (2003). All the sources within the FOV which are brighter or comparable to PKS 1830 – 211 were taken into account in extracting the source spectrum and light curve. An additional 3% systematic error was added to the spectra because of calibration uncertainties. The spectra were fitted with XSPEC v 12.3.1 and the model parameters were estimated at 90% confidence level.

The sum of all observations provide a detection with IBIS/ISGRI at $\sim 33\sigma$ level in the 20 – 100 keV energy band (Fig.1). The average 20 – 100 keV flux is 0.75 ± 0.03 counts/s, corresponding to ~ 3 mCrab, consistent with the results obtained by Bassani et al. (2006) over the first 2.5-year data.

The spectrum of the entire ISGRI data is well fit ($\tilde{\chi}^2 = 0.59$ with 8 degrees of freedom)

by a power-law model with $\Gamma = 1.29_{-0.15}^{+0.16}$ in the 20 – 250 keV energy band. We would like to note that the contribution from 150-250 keV is rather small and therefore does not affect the overall spectral fitting.

2.2. *XMM-Newton*

The *XMM-Newton* data available for PKS 1830 – 211 are three observations with the ObsID 0204580201, 0204580301 and 0204580401, carried out in March 10, 24, and April 05, 2004, respectively (Table 2). Data of EPIC-PN (Strüder et al. 2001) and EPIC-MOS (Turner et al. 2001) have been processed, screened and analyzed by using the same procedures described in Foschini et al. (2006), but with SAS v 7.1.0 with the latest calibration files as of July 16, 2007. This software version allows us to probe the lowest energy part of the spectrum (down to 0.2 keV).

The results of the fits on the individual and averaged ObsID are summarized in Table 3. The three observations show no significant flux and spectral variability; therefore, we integrated, with the FT00L `addspec`, all the MOS1, MOS2 and PN data, respectively, to obtain an average spectrum for the joint fit with ISGRI data. Although, the broken power-law and the log-parabola models can be fit with similar results in the χ^2 test, the broken power-law is slightly better and we consider this model as the best fit. The use of a ionized absorber intrinsic to the source, to model the low-energy photon deficit, gave worst results ($\tilde{\chi}^2 = 1.14$ for 1397 dof in the average spectrum). A change in χ^2 is about 130 with respect to the cold absorption shown in Table 6.

2.3. *SWIFT*

SWIFT is a γ -ray burst explorer and was launched on November 20, 2004. It carries three co-aligned detectors (Gehrels et al. 2004), namely the Burst Alert Telescope (BAT, Barthelmy et al. 2005), the X-Ray Telescope (XRT, Burrows, et al. 2005) and the Ultraviolet/Optical Telescope (UVOT, Roming et al. 2005).

BAT has rather large field of view of 1.4 sr in partially-coded mode and works in the 15 – 150 keV energy band. This makes it possible for a source to be daily monitored at the hard X-rays. The data products are therefore the source lightcurves and are publicly available¹. The BAT lightcurve traces PKS 1830 – 211 back to February 12, 2005, in the

¹See the *SWIFT*/BAT transient monitor results provided by the *SWIFT* Team at

15 – 50 keV energy band (see Fig.2). This lightcurve has a weighted-average flux value of $4.56 \pm 0.48 \times 10^{-3}$ counts $\text{cm}^{-2} \text{s}^{-1}$, corresponding to 2 mCrab at $\sim 9.5\sigma$ over a time period of roughly 2.5 years.

2.4. COMPTEL

The imaging Compton Telescope COMPTEL (1991-2000) onboard the *Compton Gamma-Ray Observatory* (CGRO) was sensitive to γ -rays in the 0.75 – 30 MeV energy range with an energy resolution of $\sim 10\%$. It had a large field of view and was able to detect γ -ray sources with an accuracy of the order of $1^\circ - 2^\circ$ (e.g., see Schönfelder et al. 1993).

The standard imaging method of maximum likelihood was applied for COMPTEL data analysis. The detection significance can be estimated from the quantity $-2 \ln \lambda$, where λ is the ratio of the likelihood L for the background and the source plus background. For a known source, $-2 \ln \lambda$ has the χ^2 distribution with 1 free parameter in addition to the null hypothesis (χ_1^2 , de Boer et al. 1992). The point spread function of the instrument is applied by assuming an E^{-2} power law shape for the input spectrum. The background is derived, with the first order of approximation, by a filter technique in data space (Bloemen et al. 1994).

PKS 1830 – 211 was marginally detected in the 1 – 3 MeV band at 4.5σ level, using the first 4-years data (Collmar 2006). Here we take the complete 6-years COMPTEL data (see Table 4), until the second reboot of the satellite in 1997, after which the background changed a lot making it difficult for further research, to investigate again the MeV emission. These data are subdivided into the so-called *CGRO* phases, with each period covering typically one year of observations. The source is again detected mainly in 1 – 3 MeV band, but the detection significance is improved to 5.2σ ($-2 \ln \lambda \sim 27$) by using two-year more data. Fig. 3 shows the sky map in 1 – 3 MeV band. The source fluxes are given in Table 5, in 4 energy bands (0.75 – 1, 1 – 3, 3 – 10 and 10 – 30 MeV, respectively).

3. Time variability

The ISGRI light curve on a scw basis shows no clear flux variability (see Fig. 4). A fit to this lightcurve with a constant results in a $\tilde{\chi}^2 \sim 0.72$. To improve the statistics, data from each observational group (totally there are 7 groups, separated by long observational gaps)

are combined to produce alternative lightcurves, as also shown in Fig. 4. The flux tends to drop smoothly during the first 2.5 years since 2003 and then to raise in the following years. A search for the flux variability on shorter time scales (4 days bins) resulted in two interesting episodes (see Fig. 5). In the first episode, the flux drops by a factor of about 6 on a time scale of about 20 days, while in the second episode (this one has low significance), the flux changed by a factor 2 on time scale of 8 days. Such excess in flux, although weak, is indicated as well in the energy bands of 20-40 keV and 40-100 keV. However, these episode events might be regarded only as hints for flux variability and the statistics is not sufficient to investigate in details these episodes.

SWIFT/BAT provides a daily lightcurve in the 15 – 50 keV energy band since February 2005. However, large error bars, mainly due to systematics, prevent us from inferring trends in flux evolution. Therefore, the data are combined in 10-days bins and the resulted lightcurve shows three time zones with persistent flux excess (see Fig. 2). Accordingly, the observations are divided again into 6 parts, over which the weighted average in flux are shown in Fig.2. This lightcurve suggests that PKS 1830 – 211 is rather variable at the hard X-rays on the time scale of months.

The lightcurves from COMPTEL (1 – 3 MeV, time period 1991 – 1997) and EGRET (\geq 100 MeV, time period 1991 – 1995) are shown in Fig. 6, with each bin presenting the average of one *CGRO* satellite observing phase. These lightcurves indicate that PKS 1830 – 211 is likely to have persistent emission over years at γ -rays.

4. Broad-band energy spectrum

We performed a joint fit of the *XMM-Newton*/*INTEGRAL* data. The results are shown in Table 6 and Fig. 7. The source luminosity in the 0.2 – 250 keV energy band is calculated as 3.5×10^{48} erg s⁻¹. We note that the fit by a simple power-law model ($\Gamma \sim 1.12$) results in a reduced $\chi^2 \sim 1.13$ under 1408 dofs. Therefore, the broken power-law model results to be again the best fit model, with an improvement with respect to the single power-law model $> 99.99\%$ as calculated with the *F*-test.

At MeV energies the spectrum can be well represented ($\tilde{\chi}^2 = 0.4$ for 2 dof) by a single power-law model with $\Gamma = 2.23^{+0.36}_{-0.27}$ measured from COMPTEL data combined from *CGRO* phases 1-4. This spectrum is then used in the followings to compare with the simultaneous EGRET one in the \geq 100 MeV energy band (Hartman et al. 1999).

Fig. 8 shows the high-energy broad-band spectrum for the results derived in this paper, including the data from *XMM-Newton* and *INTEGRAL* to cover the soft/hard X-rays (0.2 –

250 keV) energy band; from COMPTEL for the γ -rays (0.75 – 30 MeV); and from EGRET for the γ -rays in the ≥ 100 MeV energy band (Hartman et al. 1999). We considered the EGRET and COMPTEL spectra obtained simultaneously in phases 1 – 4, because they were co-aligned in pointing onboard *CGRO*.

In such a broad-band view, the power output of PKS 1830 – 211 shows a bump located at MeV energies, as expected in the common view of a high-luminosity blazar, where the high-energy part of the spectral energy distribution (SED) is due to inverse-Compton emission from the relativistic electrons in a jet scattering of seed photons coming from a source external to the jet (broad-line region, accretion disk,...; see Fossati et al. 1998, Ghisellini et al. 1998, Maraschi et al. 2008).

5. Discussion and summary

The most interesting feature in the broad-band high-energy spectrum of PKS 1830 – 211 is the spectral flattening below ~ 4 keV. Such a flattening has been observed also by De Rosa et al. (2005) in the combined *Chandra/INTEGRAL* spectrum, but the best fit model proposed is a single power-law with $\Gamma = 1.09 \pm 0.05$ extending over the entire 0.5 – 80 keV band absorbed by cold gas from the intervening galaxy at $z = 0.89$, with column density $N_{\text{H}}^z \sim 2 \times 10^{22} \text{ cm}^{-2}$. Instead, in the present work, by analyzing a spectrum covering a wider energy range (0.2 – 250 keV), we have shown evidence of a photon deficit at low energies in addition to the absorption from the intervening galaxy, confirming and extending the results obtained with *XMM-Newton* only (0.4 – 10 keV) reported by Foschini et al. (2006). This low-energy photon deficit can be best fit with a power-law harder ($\Gamma \sim 1.0$) than the one at energies greater than ~ 4 keV ($\Gamma \sim 1.3$).

This low-energy photon deficit has been often observed in high-redshift flat-spectrum radio quasars (Fiore et al. 1998; Worsley et al. 2004). According to Fiore et al. (1998), the photoelectric absorption intrinsic to the quasar is likely to be the origin of these low-energy roll-off. However, in the case of PKS 1830 – 211, the tests performed to fit with a ionized absorber the low-energy data gave worst results (see Sect. 2.2). The broken power-law is statistically required and this suggests that the spectral break is likely to be due to the intrinsic curvature of the spectrum near the low-energy end of the External-Compton (EC) component, while the relative importance of the Synchrotron Self-Compton (SSC) component is likely to decrease due to the increasing importance of the external (broad-line region, accretion disk, other) radiation field (Tavecchio et al. 2007; Ghisellini et al. 2007).

However, in the case of PKS 1830 – 211, the gravitational lensing should have an impact

on the spectral and variability properties of the source, but it is not clear how to weight it at high-energy. These effects in the γ -ray band on distant blazars have been discussed by Combi & Romero (1998) and Torres et al. (2002, 2003). The observed hard X-rays and, probably the soft X-rays as well, are the combination of the contributions from SSC and EC, which in turn are generated from different places. Therefore, the lensing can act differently, resulting in changes in spectral shape.

We can also probe further on the possible intrinsic spectrum and the amplification factor corresponding to different part of the energy spectrum of PKS 1830 – 211. We assume that, apart from the absorptions in Table 6 due to the Galactic column and the intervening system, the spectral break and roll-off in spectrum at low energies is caused by the difference in amplification factor. Therefore, we take as the intrinsic spectrum of PKS 1830 – 211 the power law with $\Gamma \sim 1.3$ from ~ 4.3 to 250 keV. We extend this value to low energies, calculate the flux in the 0.2 – 4.3 keV energy band and compare to the observed one. The ratio of the amplification factor at energies between below and above 4.3 keV is estimated by the value around 0.8. This value appears to be too low, as it is expected that the amplification factor increases with the energy and, so far, the available modelings of the magnification factor from radio/optical observations is in the range 2 – 4 (Nair et al. 1993, Swift et al. 2001, Courbin et al. 2002).

The time variability analysis could offer another way to try estimating the impact of the gravitational lensing. PKS 1830 – 211 is known to be radio variable on time scales of months (Steppe et al. 1993). Other estimations of time scales are of 44 ± 9 days (van Ommen et al. 1995) or 24 ± 2 days (Lovell et al. 1998). In modelling PKS 1830 – 211 by Subrahmanyam et al. (1990), the time lag between the two main components (NE and SW) is expressed as $\sim 6(z_g/0.1)(2h)^{-1}$ days, where z_g is the redshift of the lensing galaxy, h is the Hubble constant in units of $100 \text{ km s}^{-1} \text{ Mpc}^{-1}$. By setting the lensing galaxy at $z = 0.89$, and $h \sim 75 \text{ km s}^{-1} \text{ Mpc}^{-1}$, we have the time lag of the order of 71 days. Therefore, the time lag between the two core components might be in the range 24 – 70 days.

The hard X-ray variability displayed in the lightcurves of *INTEGRAL*/ISGRI in the 20 – 100 keV band and of *SWIFT*/BAT in the 15 – 50 keV band is quite beyond this range. The source flux can vary by a factor of 2 on time scales of months to year and the relatively poor statistics prevent us from establishing convincing evidences of the flux variability on shorter time scales. The observed variability might be the result of the evolutions either of the relativistic jet plasma or the inverse-Compton-scattered soft target photons. It might be that, by given a steady jet plasma, the soft target photons have the density evolving over months to year, which cause the long term variability showing up at hard X-rays. De Rosa et al. (2005) reproduced the SED of PKS 1830-211 with a SSC+EC model, where the

EC component was dominated by photon field from the torus. This scenario could fit with the observed hard-X ray variability on a year time scale, when this variability is attributed to the evolution of the soft photons target density. However, we point out that the SED built by De Rosa et al. (2005) has been corrected at high-energy by the amplification factor due to the gravitational lensing, which in turn is affected by large uncertainties, as we have already underlined. One of the main result of the amplification is to change the luminosity of the seed photon source and, therefore, the conclusions by De Rosa et al. (2005) could be severely biased by the not fully justified assumption of the amplification factor correction. A possible measurement of a time lag at hard X-rays in the future may help to resolve the contribution, if any, of the core region to the jet dominated emission.

An indication might be that, as already pointed out in De Rosa et al. (2005), PKS 1830–211 is actually another blazar to have persistent MeV emissions, which are always detectable by COMPTEL. The other two COMPTEL blazars which own MeV emission be visible over years are 3C 273 (Collmar et al. 2000) and 3C 354.3 (Zhang et al. 2005). Such a long-term steady MeV emission has been discussed in Zhang et al. (2005) for 3C 454.3, in the framework of leptonic multicomponent models where the MeV emission might be dominated by EC of seed photons coming directly from the accretion disk. The bulk Lorentz factor is argued to keep at a relatively high level to maintain the MeV emission visible over the time scale of years. In the case of PKS 1830 – 211, such a bulk Lorentz factor has been estimated to be about 17 by Foschini et al. (2006), where – given the uncertainties of the lensing at high-energies – the modelling of the SED was performed on the observed data, without any correction.

In summary, we presented here the most updated broad-band high-energy spectrum of PKS 1830 – 211. The source presents a low-energy roll-off that can be explained efficiently in term of natural interplay between SSC and EC, as shown in other high- z FSRQ. However, it is not clear what is the weight of the amplification factor due to the gravitational lensing. Future observations at X-rays with higher spatial resolution should allow us to measure this factor.

We thank the anonymous referee for the constructive comments that were of great help in improving our paper. This work was subsidized by the National Natural Science Foundation of China, and the CAS key Project KJCX2-YW-T03. DFT acknowledges support by Spanish MEC grant AYA 2006-00530 and CSIC grant PIE 200750I029. J.-M. W. thanks the Natural Science Foundation of China for support via NSFC-10325313, 10521001 and 10733010. LF acknowledges support by ASI/INAF contract I/088/06/0.

REFERENCES

- Barthelmy, S.D., Barbier, L.M., Cummings, J.R., et al. 2005, *Space Sci. Rev.*, 120, 143
- Bassani, L., Molina, M., Malizia, A., , et al. 2006, *ApJ*, 636, L65
- Beckmann, V., Gehrels, N., Shrader, C., R., et al. 2006, *ApJ*, 638,642
- Bloemen, H., Hermsen, W. & Swanenburg, B. N., 1994, *ApJS*, 92, 419
- Burrows, D.N., David, N., Hill, J.E., et al. 2005, *Space Sci. Rev.*, 120, 165
- Collmar, W. 2006, *ASPC*, 350, 120
- Collmar, W., Reimer, O., Bennett, K., et al. 2000, *A&A*, 354, 513
- Combi J.A. & Romero G. E. 1998, *A&AS* 128, 423
- Courbin, F., Meylan, G., Kneib, J.P., & Lidman, C. 2002, *ApJ*, 575, 95
- de Boer, H., Bennett, K., den Herder, H., et al. 1992, in *Data Analysis in Astronomy IV*, ed. V. Di Gesù, L. Scarsi, R. Buccheri, et al. (New York: Plenum Press), 241
- De Rosa, A., Piro, L., Tramacere, A., et al. 2005, *A&A*, 438, 121
- Fiore, F., Elvis, M., Giommi, P. & Padovani, P., 1998, *ApJ*, 492, 79
- Foschini, L., Ghisellini, G., Raiteri, C.M., et al. 2006, *A&A*, 453, 829
- Fossati, G., Maraschi, L., Celotti, A., Comastri, A. & Ghisellini, G., 1998, *MNRAS*, 299, 433
- Gehrels, H., Chincarini, G., Giommi, P., et al. 2004, *ApJ*, 611, 1005
- Ghisellini, G., Celotti, A., Fossati, G., Maraschi, L. & Comastri, A., 1998, *MNRAS*, 301, 451
- Ghisellini, G., Foschini, L., Tavecchio, F. & Pian, E. 2007, *MNRAS*, 382, L82
- Goldwurm, A., David, P., Foschini, L., et al., 2003, *A&A*, 411, L223
- Hartman, R. C., Bertsch, D. L., Bloom, S. D., et al., 1999, *ApJS*, 123, 79
- Kalberla, P. M. W., et al., 2005, *A&A*, 440, 775
- Jauncey, D. L., Reynolds, J. E., Tzioumis, A. K., et al. 1991, *Nature*, 352, 132

- Lebrun, F., Leray, J.P., Lavocat, P., et al. 2003, *A&A*, 411, L141
- Lovell, J. E. J., Jauncey, D. L., et al. 1998, *ApJ*, 508, 51
- Lund, N., Budtz-Jørgensen, C., Westergaard, N.J., et al. 2003, *A&A*, 411, L231
- Maraschi, L., Ghisellini, G., Tavecchio, F., Foschini, L. & Sambruna, R. M., 2008, Proceedings of the Conference “High-Energy Processes in Relativistic Outflows”, Dublin, September 2007 ([arXiv.org:0802.1789](https://arxiv.org/abs/0802.1789))
- Mas-Hesse, J.M., Giménez, A., Culhane, J.L., et al. 2003, *A&A*, 411, L261
- Mathur, S., & Nair, S., 1997, *ApJ*, 484, 140
- Nair, S., Narasimha, D., & Rao, A. P., 1993, *ApJ*, 407, 46
- Oshima, T., Mitsuda, K., & Ota, N., et al. 2001, *ApJ*, 551, 929
- Pramesh Rao A. & Subrahmanyan R., 1988, *MNRAS* 231, 229
- Roming, P.W.A., Kennedy, T.E., Mason, K.O., et al. 2005, *Space Sci. Rev.*, 120, 95
- Schneider, P., Ehlers, J. & Falco, E.E., 1992, *Gravitational lenses*, Springer: New York
- Schönfelder, V., Bennett, K., Bloemen, H., et al. 1993, *ApJS*, 86, 657
- Spergel, D.N., Bean, R., et al. 2007, *ApJS*, 170, 377
- Steppe, H., Paubert, G., & Sievers, A., 1993, *A&AS*, 102, 611
- Strüder, L., Briel, U., Dennerl, K., et al., 2001, *A&A*, 365, L18s
- Subrahmanyan, R., Narasimha, D., Rao, A., & Swarup, G., 1990, *MNRAS*, 246, 263
- Swift, J.J., Welch, W.J. & Frye, B.L., 2001, *ApJ*, 549, L29
- Tavecchio, F., Maraschi, L., Ghisellini, G., et al. 2007, *ApJ*, 665,980
- Torres, D. F., Romero, G. E. & Eiroa, E., 2002, *ApJ*, 569, 600
- Torres, D. F., Romero, G. E., Eiroa, E. F., Wambsganss, J., & Pessah, M. E., 2003, *MNRAS*, 339, 335
- Turner, M.J., Abbey, A., Arnaud, M., et al., 2001, *A&A*, 365, L27
- Ubertini, P., Lebrun, F., Di Cocco, G., et al., 2003, *A&A*, 411, L131

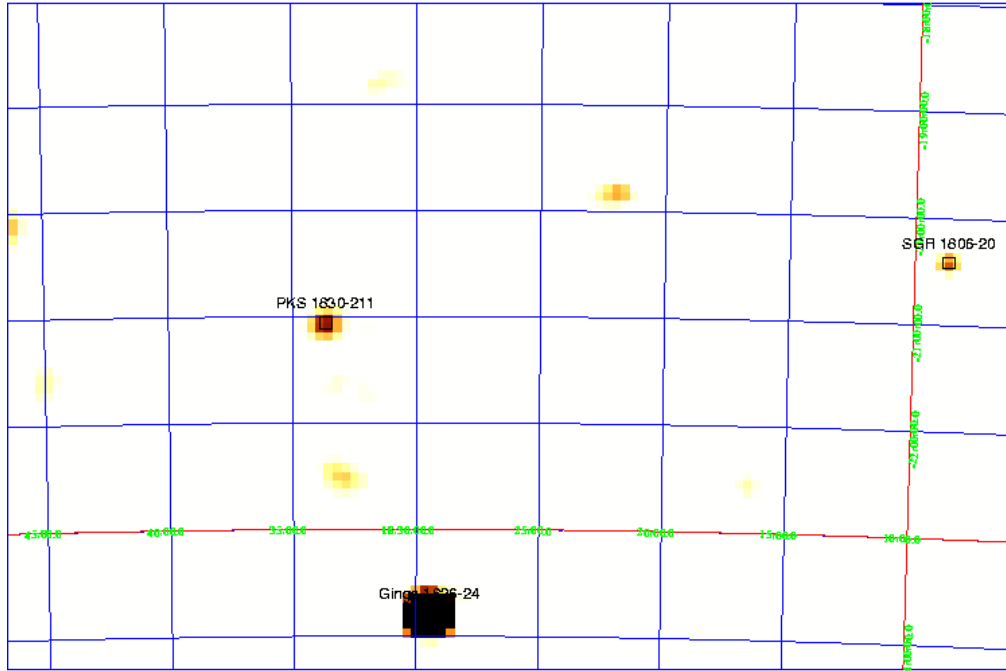


Fig. 1.— The ISGRI significance map of PKS 1830 – 211 region in the 20 – 100 keV band, obtained by combining the observations of 2003 – 2006.

van Ommen, T. D., & Jones, D. L., 1995, *ApJ*, 444, 561

Vedrenne, G., Roques, J.-P., Schönfelder, V., et al., 2003, *A&A*, 411, L63

Walsh, D., Carswell, R. F., & Weymann, R. J., 1979, *Nature*, 279, 381

Worsley, M.A., Fabian, A.C., Turner, A.K., Celotti, A., Iwasawa, K., 2004, *MNRAS*, 350, 207

Zhang, S., Collmar, W., Schönfelder, V., 2005, *A&A*, 444, 767

Table 1: *INTEGRAL*/ISGRI observation log of PKS 1830 – 211. The revolution ID, time in MJD, number of science windows, and the total exposure are given.

Revolution ID	MJD	Number of SCW	Exposure (ks)
050-065	52710-52767	138	250.9
105-122	52875-52927	247	585.1
164-186	53052-53119	108	205.9
225-249	53234-53305	161	388.3
286-310	53417-53488	97	192.1
348-371	53602-53672	209	609.1
407-432	53777-53854	135	266.1

Table 2: *XMM-Newton* observation log of PKS 1830 – 211. The observational ID, time in calendar date and MJD, prime observational target, the pointing offset angle and total exposure are given.

ID	Date (dd/mm/yy)	MJD	Object	Offset angle arcsecond	Exposure* ks
0204580201	10/03/2004	53074	PKS 1830-211	1.1	3,7,7
0204580301	24/03/2004	53088	PKS 1830-211	1.1	27,31,31
0204580401	05/04/2004	53100	PKS 1830-211	1.1	13,19,19

* Effective exposure on PN, MOS1, and MOS2, respectively, after having removed periods with high background.

Table 3: Summary of the results of the individual fits on *XMM-Newton* data. In all the three models we fixed the Galactic column to $N_{\text{H}} = 2.05 \times 10^{21} \text{ cm}^{-2}$ and we left free an absorption redshifted to the value of the intervening galaxy ($z = 0.89$); the value is in [10^{22} cm^{-2}]. The continuum of the blazar is modeled with a redshifted power-law or with a broken power-law or with a log-parabola, according to the formula $F(E) = E^{[-a-b \log(E)]}$, where a is the initial photon index and b is the curvature parameter. The break energy is in [keV]. N is the flux density given at 1 keV in units of [$10^{-3} \text{ ph cm}^{-2} \text{ s}^{-1} \text{ keV}^{-1}$]; F is the observed flux in the 0.2 – 10 keV band in units [$10^{-11} \text{ erg cm}^{-2} \text{ s}^{-1}$].

Redshifted Power-Law							
ObsID	N_{H}^z	Γ		N	$\tilde{\chi}^2/\text{dof}$	F	
0204580201	2.5 ± 0.2	1.14 ± 0.04		5.9 ± 0.7	1.06/427	1.48	
0204580301	2.5 ± 0.1	1.12 ± 0.02		5.2 ± 0.3	1.08/1340	1.38	
0204580401	2.2 ± 0.1	$1.12^{+0.03}_{-0.02}$		$4.7^{+0.4}_{-0.3}$	1.02/867	1.27	
Broken Power-Law							
ObsID	N_{H}^z	Γ_1	Γ_2	E_{break}	N	$\tilde{\chi}^2/\text{dof}$	F
0204580201	$2.0^{+0.1}_{-0.3}$	$0.95^{+0.09}_{-0.13}$	1.46 ± 0.17	$4.1^{+0.6}_{-0.7}$	1.2 ± 0.1	0.99/425	1.43
0204580301	$1.9^{+0.2}_{-0.1}$	0.88 ± 0.07	$1.26^{+0.06}_{-0.04}$	$3.3^{+0.4}_{-0.3}$	$1.01^{+0.07}_{-0.06}$	1.03/1338	1.36
0204580401	$1.98^{+0.16}_{-0.07}$	$1.00^{+0.06}_{-0.03}$	$1.33^{+0.19}_{-0.06}$	$4.3^{+0.8}_{-0.2}$	$1.03^{+0.07}_{-0.03}$	0.99/865	1.24
Broken Power-Law (average)*							
	2.10 ± 0.04	$1.000^{+0.001}_{-0.018}$	$1.33^{+0.03}_{-0.04}$	$4.26^{+0.21}_{-0.12}$	$1.121^{+0.004}_{-0.035}$	1.04/1397	1.34
Log-parabola							
ObsID	N_{H}^z	a	b		N	$\tilde{\chi}^2/\text{dof}$	F
0204580201	1.2 ± 0.4	< 0.5	0.77 ± 0.21		$0.80^{+0.15}_{-0.12}$	0.98/426	1.41
0204580301	1.5 ± 0.2	0.43 ± 0.12	0.57 ± 0.10		0.81 ± 0.06	1.02/1339	1.34
0204580401	$1.5^{+0.3}_{-0.2}$	$0.58^{+0.21}_{-0.11}$	$0.45^{+0.17}_{-0.09}$		$0.83^{+0.12}_{-0.06}$	0.99/866	1.26

* The average spectrum has been rebinned in order to have at least 50 counts per bin. The PN has been considered as reference detector and the intercalibration constants are: MOS1/PN= 1.21 ± 0.01 and MOS2/PN= 1.23 ± 0.01 .

Table 4: COMPTEL observations of the sky region of PKS 1830 – 211 during 1991 – 1997. The CGRO VPs, their time periods in calendar date and MJD, prime observational targets of *CGRO*, and the pointing offset angle are given.

VP	Date (dd/mm/yy)	MJD	Object	Offset angle	CGRO Phase	
5.0	12/07/91-26/07/91	48449-48463	Gal. Center	12°	Phase I	
7.5	15/08/91-22/08/91	48483-48490	Gal 025-14	15°		
13.0	31/10/91-07/11/91	48560-48567	GAL 025-14	15°		
16.0	12/12/91-27/12/91	48602-48617	SCO X-1	29°		
20.0	06/02/92-20/02/92	48658-48672	SS 433	28°		
27.0	28/04/92-07/05/92	48740-48749	4U 1543-47	41°		
35.0	06/08/92-11/08/92	48840-48845	ESO 141-55	41°		
38.0	27/08/92-01/09/92	48861-48866	ESO 141-55	41°		
42.0	15/10/92-29/10/92	48910-48924	PKS 2155-304	40°		
43.0	29/10/92-03/11/92	48924-48929	MRK 509	29°		
209.0	09/02/93-22/02/93	49027-49040	2CG010-31	30°	Phase II	
210.0	22/02/93-25/02/93	49040-49043	Gal. Center	20°		
214.0	29/03/93-01/04/93	49075-49078	Gal. Center	20°		
219.4	05/05/93-06/05/93	49112-49113	Gal. Center	31°		
223.0	31/05/93-03/06/93	49138-49141	Gal. Center	14°		
226.0	19/06/93-29/06/93	49157-49167	Gal. 355+5	20°		
231.0	03/08/93-10/08/93	49202-49209	NGC 6814	12°		
229.0	10/08/93-11/08/93	49209-49210	Gal. 5+05	13°		
229.5	12/08/93-17/08/93	49211-49216	Gal. 5+05	13°		
232.0	24/08/93-26/08/93	49223-49225	Gal. 348-00	25°		
232.5	26/08/93-07/09/93	49225-49237	Gal. 348-00	25°		
302.3	09/09/93-21/09/93	49239-49251	GX 1+4	18°		
323.0	22/03/94-05/04/94	49433-49447	Gal. 357-112	16°		
324.0	19/04/94-26/04/94	49461-49468	Gal. 016+05	12°		
330.0	10/06/94-26/04/94	49513-49517	Gal. 018+00	8°		
332.0	18/06/94-05/07/94	49521-49538	Gal. 018+00	8°		
334.0	18/07/94-25/07/94	49551-49558	Gal. 009-08	4°		
336.5	04/08/94-09/08/94	49568-49573	GRO J1655-40	33°		
338.0	29/08/94-31/08/94	49593-49595	GRO J1655-40	28°		
339.0	20/09/94-04/10/94	49615-49629	3C 317	47°		
414.3	29/03/95-04/04/95	49805-49811	GRO J1655-40	26°	Phase IV	
421.0	06/06/95-13/06/95	49874-49881	Gal. Center	18°		
422.0	13/06/95-20/06/95	49881-49888	Gal. Center	18°		
423.0	20/06/95-30/06/95	49888-49898	Gal. Center	11°		
423.5	30/06/95-10/07/95	49898-49908	PKS 1622-297	32°		
429.0	20/09/95-27/09/95	49980-49987	GAL 018+04	11°		
501.0	03/10/95-17/10/95	49993-50007	GAL 28+4	18°		
508.0	14/12/95-20/12/95	50065-50071	GAL 5+0	9°	Phase V	
509.0	20/12/95-02/01/96	50071-50084	GAL 21+14	21°		
513.0	06/02/96-13/02/96	50119-50126	PKS 2155-304	47°		
516.1	18/03/96-21/03/96	50160-50163	GRO J1655-40	33°		
520.4	21/05/96-28/05/96	50224-50231	PKS 2155-304	47°		
524.0	09/07/96-23/07/96	50273-50287	GX 339-4	29°		
529.5	27/08/96-06/09/96	50322-50332	GRO J1655-40	28°		
624.1	04/02/97-11/02/97	50483-50490	Gal 16+00	10°		Phase VI
619.2	14/05/97-20/05/97	50582-50588	GRS 1915+105	35°		
620.0	10/06/97-17/06/97	50609-50616	Gal 16+04	10°		
625.0	05/08/97-19/08/97	50665-50679	GRS 1758-258	13°		
615.1	19/08/97-26/08/97	50679-50686	PKS 1622-297	30°		

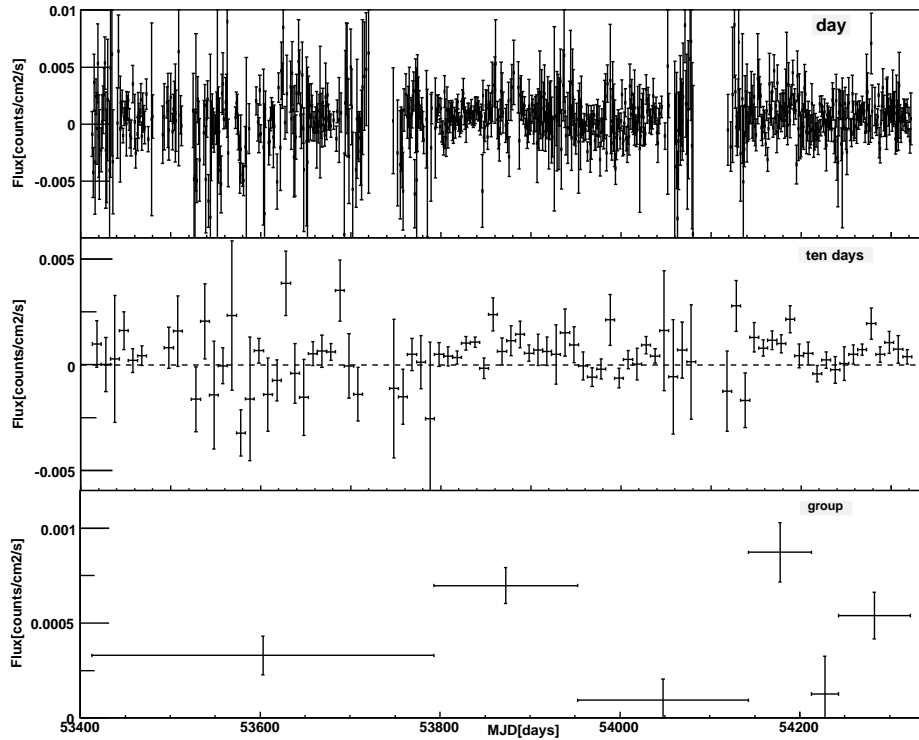


Fig. 2.— *SWIFT* light curves (15 – 50 keV) with each bin representing a time scale of one day (top), ten days (middle) and an observational group (bottom). The observational groups are defined to have persistent emission excess as showing up in the lightcurve of the ten-day basis (the middle panel).

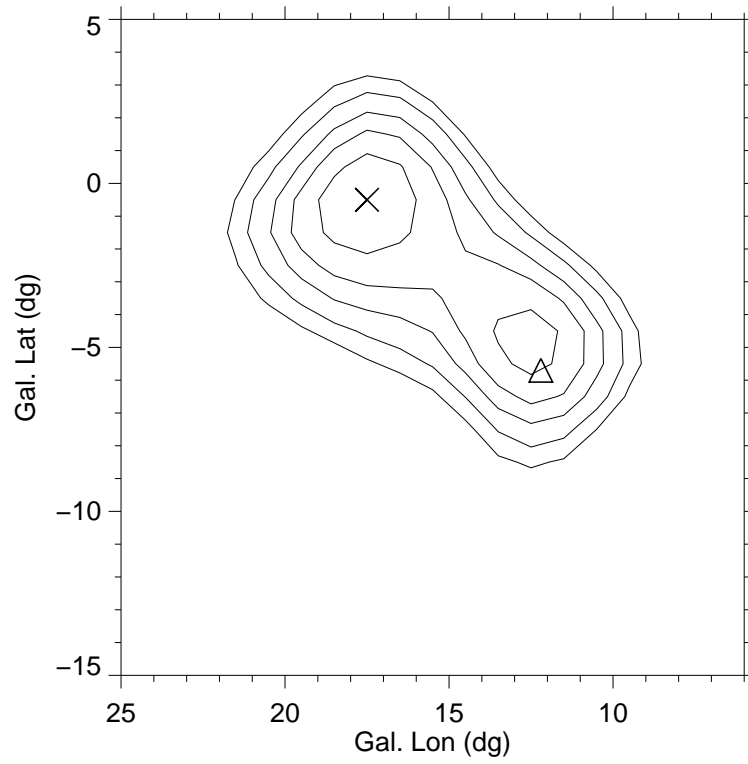


Fig. 3.— The 1 – 3 MeV map from COMPTEL observations of phases 1 – 6. The contours start at detection significance level of 3σ , with the step of 1σ . The symbols of the triangle represent the location of PKS 1830 – 211, and the cross the location of the so-called MeV source $l = 18$.

Table 5: Fluxes of PKS 1830 – 211 and the time periods of COMPTEL observations are listed. The error bars are 1σ .

Period	MJD	Flux (10^{-5} ph cm $^{-2}$ s $^{-1}$)			
		0.75-1 MeV	1-3 MeV	3-10 MeV	10-30 MeV
Phase 1-6	48392-50539	4.9 ± 1.4	7.6 ± 1.4	1.5 ± 0.6	0.4 ± 0.3

Table 6: Results of the joint *XMM-Newton/INTEGRAL* data (0.2 – 250 keV) fit with a broken power-law model plus two absorption components. Absorption columns are in units [10^{22} cm $^{-2}$]; the break energy is in [keV]; the normalization N is in [10^{-3} ph cm $^{-2}$ s $^{-1}$ keV $^{-1}$]. The intercalibration constant between EPIC-PN and ISGRI is $\text{ISGRI/PN} = 0.63\pm 0.07$.

wabs	zwabs		bknpow				$\tilde{\chi}^2/\text{dof}$
N_H	N_H	z	Γ_1	E_{break}	Γ_2	N	
0.205 (fix)	1.96 ± 0.09	0.886 (fix)	$0.93^{+0.04}_{-0.03}$	$3.68^{+0.29}_{-0.19}$	1.29 ± 0.04	1.05 ± 0.04	1.04/1406

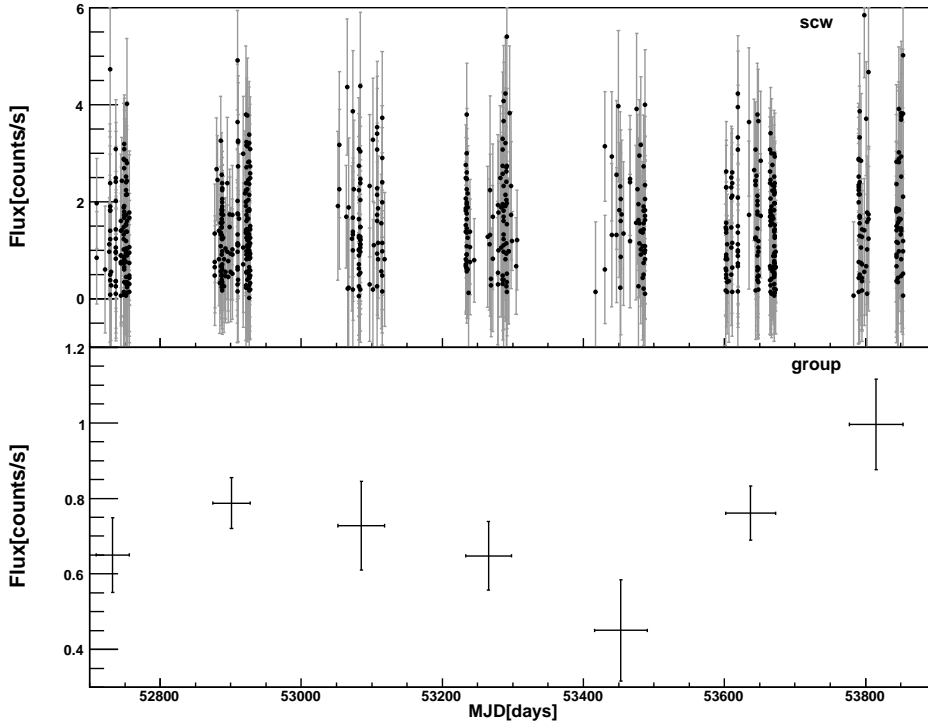


Fig. 4.— ISGRI light curves in the 20–100 keV band, on basis of scw (top) and observational group (bottom), for the time period between 2003 and 2006.

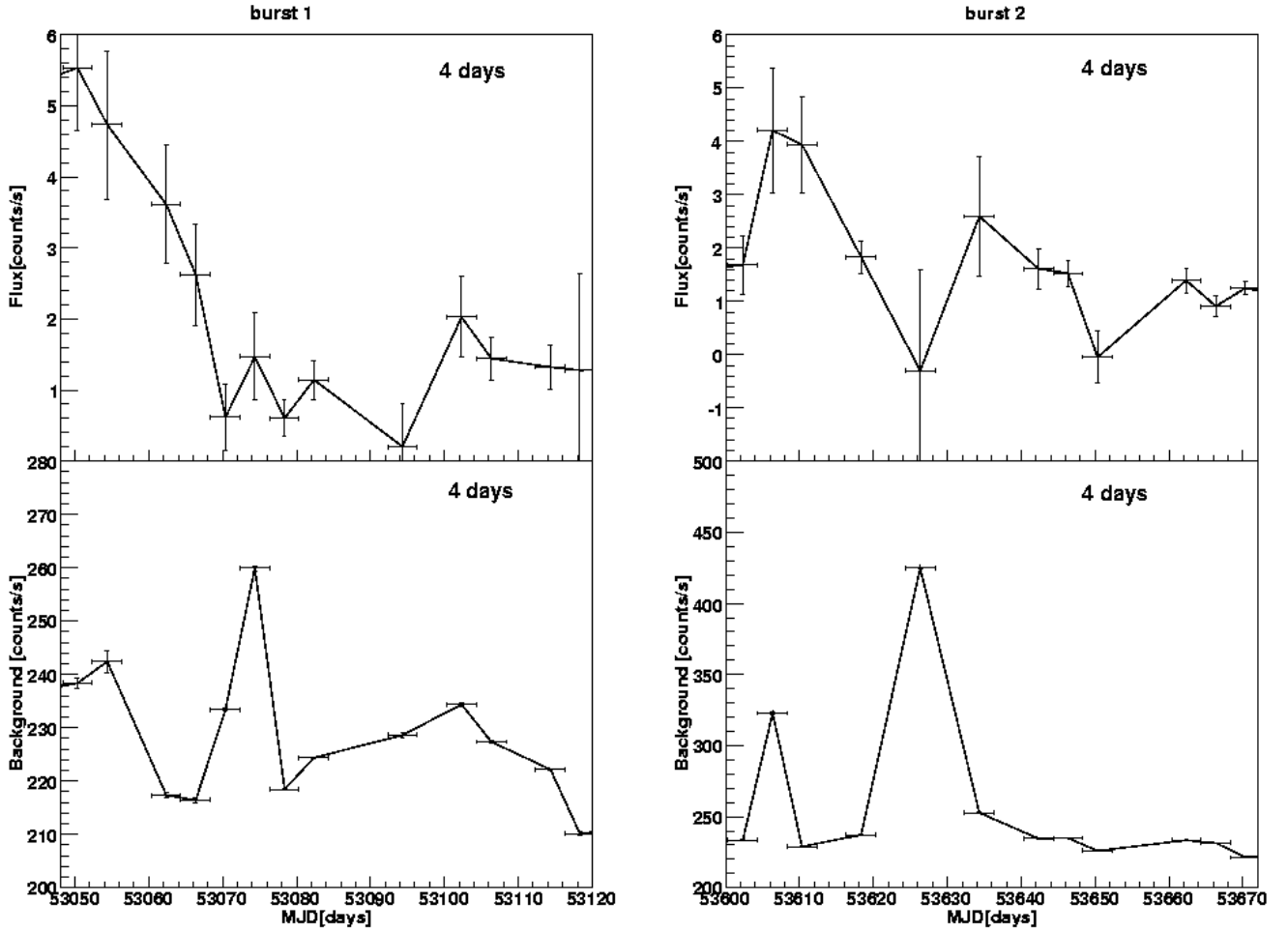


Fig. 5.— Two high-variability episodes detected by ISGRI in the 20 – 100 keV energy band, with each bin representing 4 days. The lower panels show the corresponding background light curves.

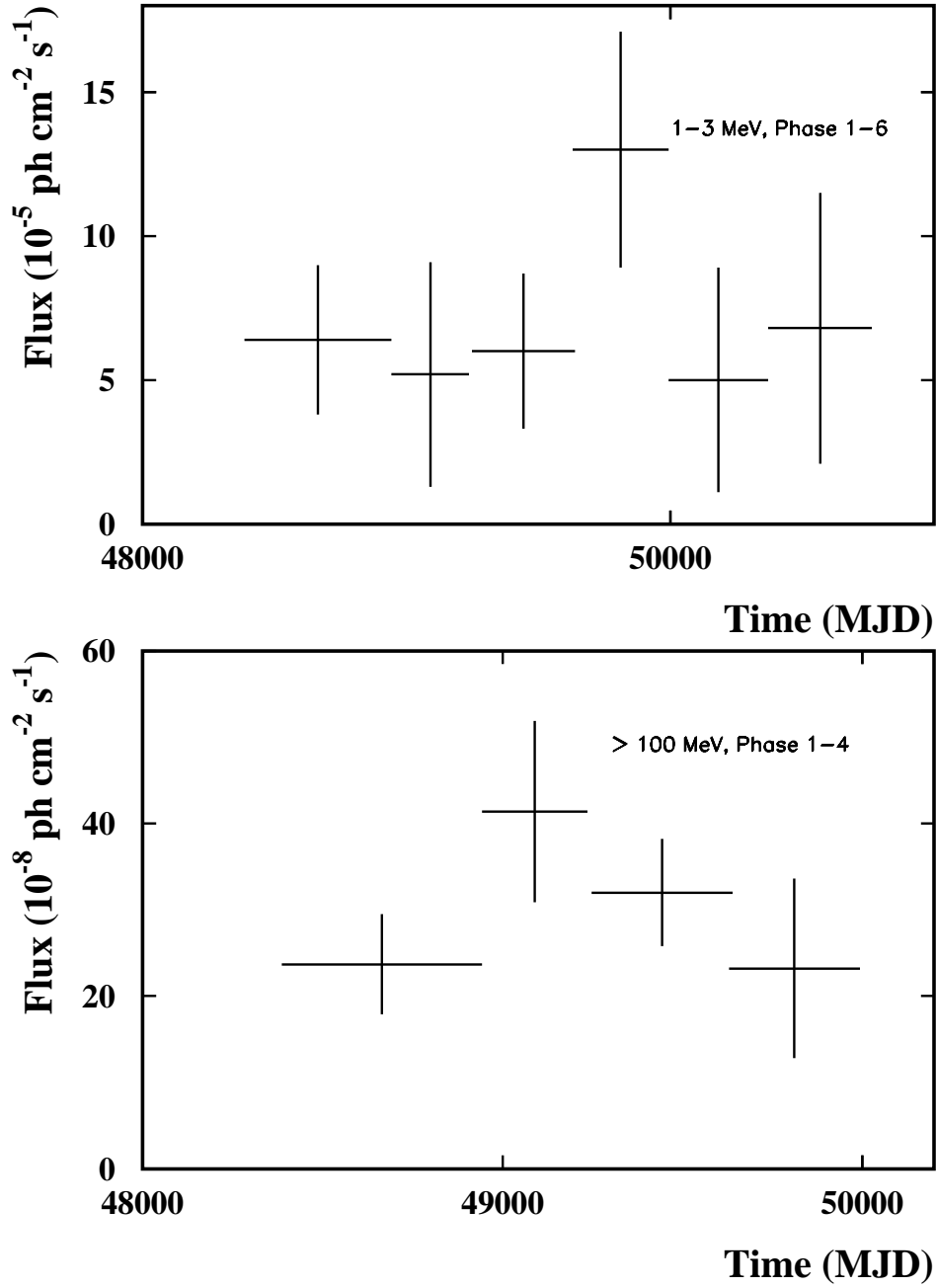


Fig. 6.— COMPTEL (upper panel) and EGRET (lower panel) lightcurves with each bin averaged over one *CGRO* phase. The error bars are 1σ .

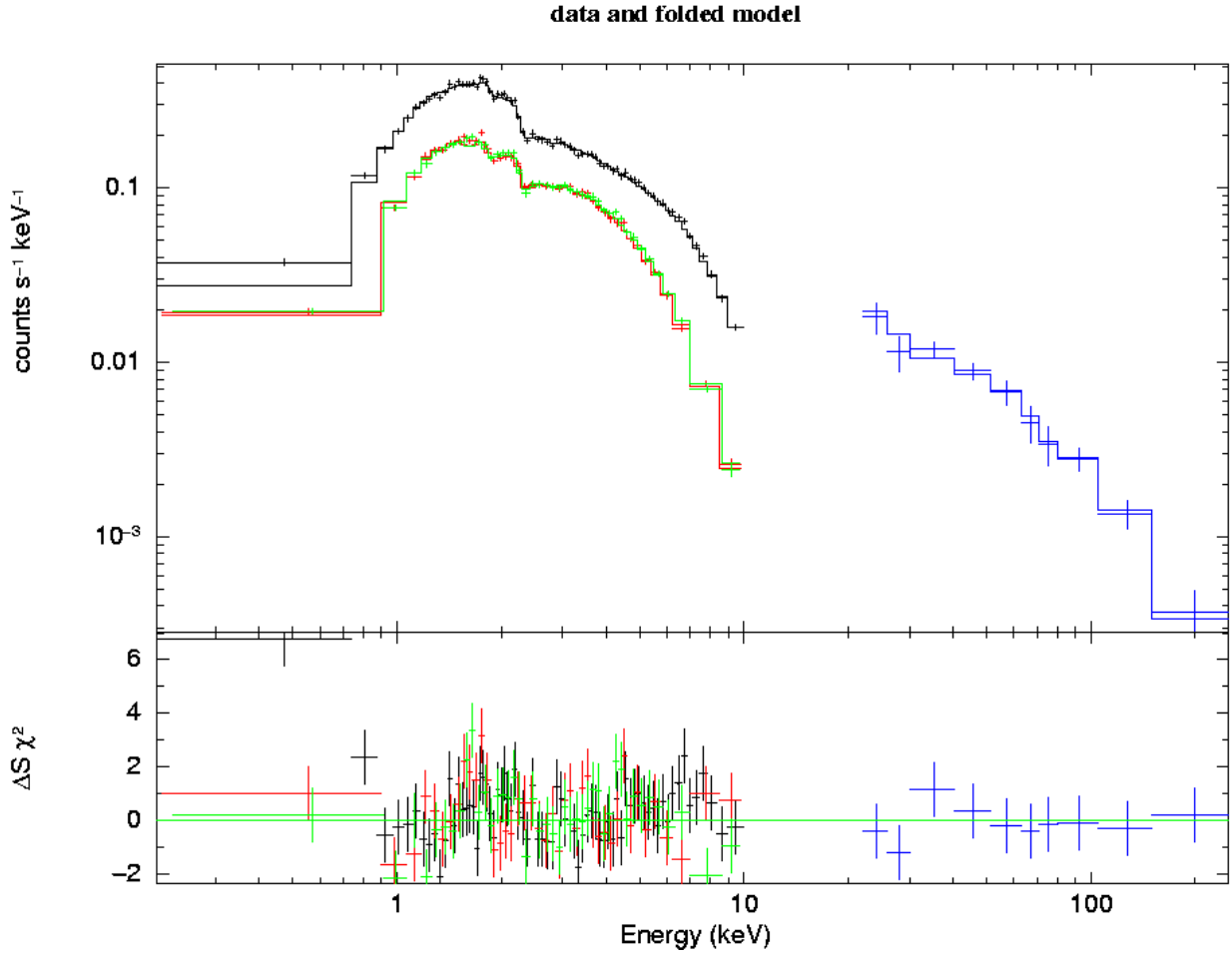


Fig. 7.— Spectral fit with a broken power law model for the combined *XMM-Newton* data (at energy below 10 keV), and the ISGRI data (at energy above 20 keV). For better visibility the *XMM-Newton* spectra have been rebinned in the plot.

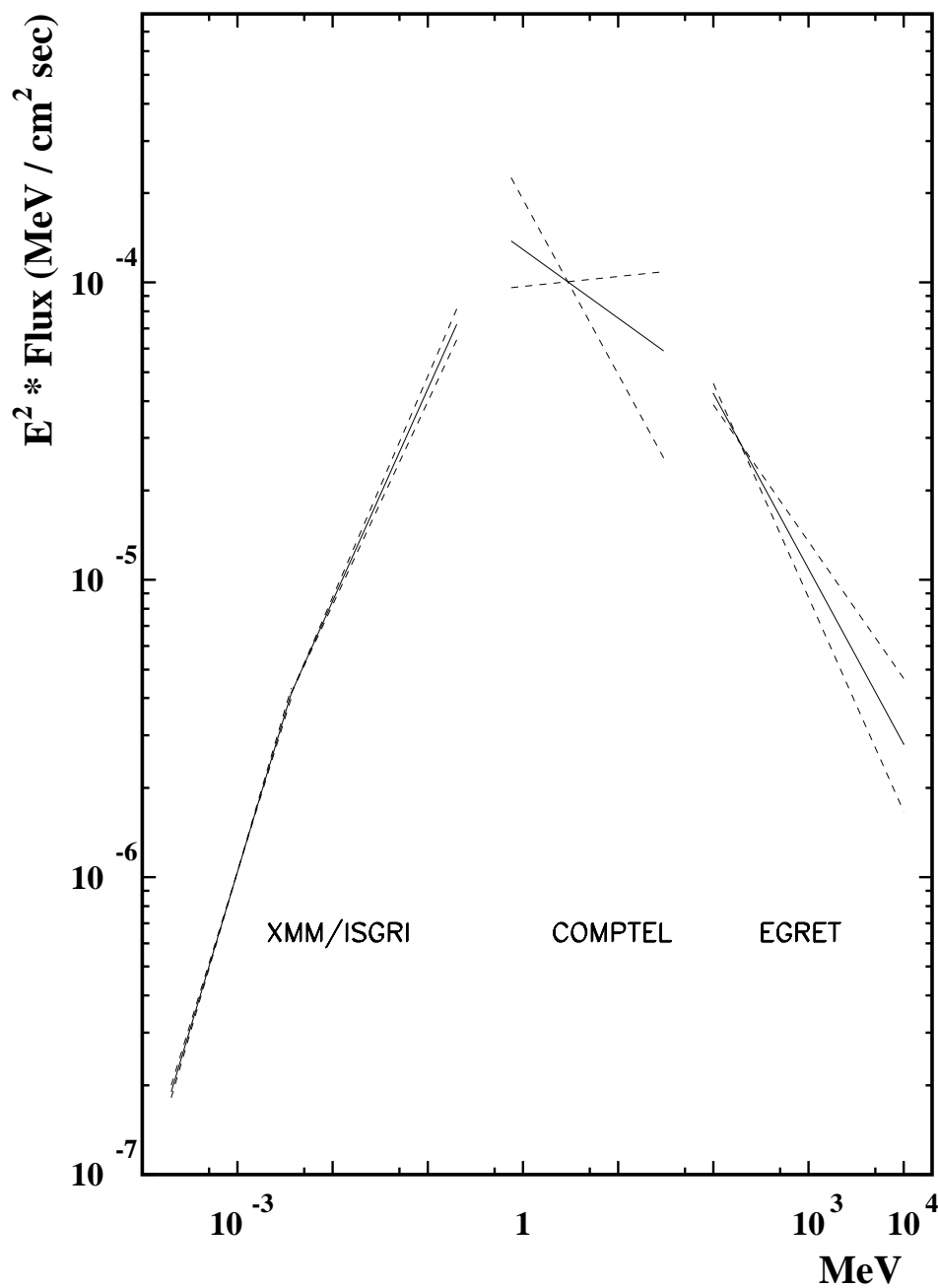


Fig. 8.— The broad energy spectrum of PKS 1830 – 211. The solid lines are the broken power law shape as obtained by *XMM-Newton/INTEGRAL* at X-rays, power law shapes by COMPTEL at MeV energies, and by EGRET at ≥ 100 MeV (Hartman et al., 1999). The dashed lines are the plots of the 1σ error in spectral shape.